A Portable 28-GHz Channel Sounder Platform and Measurement Results From Close-to-Ground Field Tests

EDWARD A. BALL (Member, IEEE), AND **SUMIN DAVID JOSEPH**

Department of Electronic and Electrical Engineering, The University of Sheffield, S10 2TN Sheffield, U.K.

CORRESPONDING AUTHOR: E. A. BALL (e-mail: e.a.ball@sheffield.ac.uk)

This work was supported by UKRI under Grant MR/T043164/1.

ABSTRACT This article describes a novel, bespoke, and low-cost 28-GHz RF TX and RX front end design that has been combined with a commercial Software-Defined Radio and Raspberry Pi controller to realize a portable propagation measurement system for the 28-GHz band. The complete sounder system can resolve an impulse from RX powers down to -107 dBm (3-dB impulse SNR) and the sounder TX can generate a signal of -8 dBm. Therefore, using 20-dBi antennas supports path-loss (PL) measurements of 139 dB. The sounder can resolve time-domain reflections to 33 ns in a channel measurement bandwidth of 60 MHz, producing both time-domain and frequency-domain results. The complete sounding system has been used to perform close-to-ground RF channel measurements, with propagation loss models and time-domain impulses extracted. Close-to-ground measurement is an underreported area of propagation research that is relevant for novel use-cases, such as in military applications or for mobile device-to-device communications. A key initial finding from the trials is that the PLs for 28-GHz indoor and outdoor links at circa 70 cm above ground seem close to that of free space, with very few strong reflections with delays exceeding 33 ns.

INDEX TERMS Measurement, millimeter-wave circuits, radio propagation, signal processing, transceivers.

I. INTRODUCTION

THE RISE of 5G has shown the huge appetite for improved communication systems, underpinned by enhanced radio technology. With the number of 5G connections predicted to reach 1.3 billion by end of 2022 and reach 4.8 billion by end of 2026 [1], the pressure on radio resources will only increase with time.

A key part of designing a viable and efficient radio system is to fully understand the radio channel in the target deployment use case. This relies on measurements and models for the channel propagation characteristics. Often, the systems used to perform such channel measurements use traditional (and costly) RF lab equipment. Mobility, power, and equipment cost issues limit their suitability in challenging use cases, where damage may result. In the past, novel propagation measurement systems using lower cost hardware have been described, such as for IoT applications in the VHF and UHF bands reporting path loss (PL) and delay spread [2], [3], [4].

At mmWave frequencies, the required measurement equipment becomes very expensive and heavy, though many valuable works have been reported using lab equipment and hybrid systems. For example, Rappaport et al. [5] presented one of the early reports on 5G channel models and propagation experiments across the mmWave bands. However, such systems are often large and costly, thus out of reach for many researchers, impeding innovation. In recent years, commercial chip manufacturers have brought to production a range of mmWave RF chips in surface mount packaging. It is the availability of these chips (as opposed to bare dies) that has led to the work described in this article; leading to a low-cost, battery-powered, portable RF mmWave transceiver platform that is suitable for general use and specifically used here for 28-GHz channel sounding.

An area of interest for mmWave channel measurements is the performance of the radio channel when close-to-ground, both outdoors and indoors. This could represent future mobile to mobile use cases in commercial communications. It is also relevant for future battlefield communications, where the high bandwidth (BW) and narrow beams can be attractive for minimizing eavesdropping or interception, while handling large amounts of data over long distance.

The main contributions of this article are as follows.

1) The development of a low-cost, battery-powered, and easily portable self-contained channel sounder system for the 28-GHz band (external band pass filter (BPF) defined range 27.5–29.5 GHz), capable of reporting PL and delay spread for PLs up to 142 dB (0-dB impulse SNR). The developed RF PCB design is presented and made available for others to copy and use [6].
2) Example measurement of 28-GHz channel responses close to ground in an indoor office environment.
3) Example measurement of 28-GHz channel responses close to ground over a 1-km outdoor scenario.
4) Extracted PL models for the measured scenarios are provided.

Section II presents related works and Section III introduces the system and RF hardware design. Section IV presents the channel sounder algorithms. System verification tests are discussed in Section V. Indoor and outdoor field test results and models are presented in Section VI. System and measurement findings are discussed in Section VII. This article concludes in Section VIII.

II. RELATED WORKS

Previously, some researchers have used vector network analyzers (VNAs) for channel measurements. Wang et al. [7] used a VNA at 38–40 GHz with external power amplifier (PA) and low noise amplifier (LNA), providing measured results to 15 m. However, as might be anticipated, these systems are limited by cable link requirements. Some authors have used fibre optic links to extend the testable distance of the VNA [8].

There have been some reported development and associated results for portable multiband systems, such as [9] operating in ISM and 60-GHz bands and using FMCW sounding signals. The Ettus Research USRP portfolio are popular systems for software-defined radio (SDR) platforms. In [10], a USRP-N210 is used for indoor channel measurements at 2.2 GHz, with 12.5-MHz sounding BW and 80-ns delay resolution. By using multiple overlapping tones, a 100-MHz total measurement BW and 10-ns delay resolution is supported.

In [11], various 28-GHz indoor channels are measured using a pseudo noise (PN) sequence at 250 Mchip/s and using commercial mmWave upconverter modules, boards, and lab equipment carried on a trolley. Results for indoor PL (log-normal models), delay spread, and angle of arrival are presented. Samimi et al. [12], Zhao et al. [13],

and Azar et al. [14] have performed extensive outdoor measurements at 28 GHz (and above), with antennas on rooftops and using sliding correlator techniques with mains powered lab equipment. A free space PL (FSPL) reference distance of 5 m was used, and log normal shadowing models are used to fit the data. Lee et al. [15] described urban microcellular channel measurements at 28 GHz with a 170-dB PL measurement capability. The transmitter was mounted on a vehicle and the receiver on a lab trolley. A continuous-wave (CW)-based channel sounder was used in [16] to perform urban canyon and rooftop propagation measurements. A measurable 28-GHz PL of up to 171 dB is reported, using a rotating horn receiver. Measurements at up to 800 m were made.

In [17], lab equipment, including an arbitrary waveform generator, is used to create a PN sounding system with 1-ns multipath resolution. This is used to measure room reflections in line-of-sight (LoS) scenarios using a steerable TX horn and omnidirectional RX. LoS tests showed similar PL to FSPL predictions, but off-axis measurements showed significant reflections from indoor surfaces. It was also found that RMS delay spread of under 30 ns were common.

Corridor measurements are performed at mmWave frequencies in [18] using lab test equipment and 1 Gchip/s PN chip rate. PL exponents were found to be significantly lower than FSPL due to wave-guiding effects of the corridor. The RMS angular spread is also found to be up to 100°. Many studies have investigated the propagation in office and university campus buildings [19], often using high performance lab RF test equipment [20]. Zhang et al. [21] found a close link between room size and model extracted parameters and report delay spreads of 11.8–83.8 ns. In general, log-normal modeling has been used at 28 GHz, such as by [22] with 5-m reference distance and [23] with 1-m reference distance, though the floating intercept PL model is also used [24].

In [25], extensive measurements of 28-GHz propagation PL, delay spread, and angular spread of arrival were made in stadiums, subways, factories, and agricultural barns. In LoS tests, in all settings, they observed close to FSPL links. For PL and angular profile channel measurements, CW was used and orthogonal frequency-division multiplexing (OFDM) was used for delay spread measurements (100-MHz BW). Measurement equipment was mobile on three trolleys and used lab test kit.

Ko et al. [26] used a 250 Mchip/s pseudo random binary sequence (PRBS)-based system at 28 GHz to measure the propagation in residential environments with foliage and vegetation. TX and RX systems are cable-linked for synchronization and a 145-dB PL measurement capability is reported. The authors report that in addition to expected floor reflections, building walls and tree foliage also lead to significant clusters of delay spread. Du et al. [27] performed suburban residential area Fixed Wireless Access scenario propagation measurements at 28 GHz at up to 200 m. CW
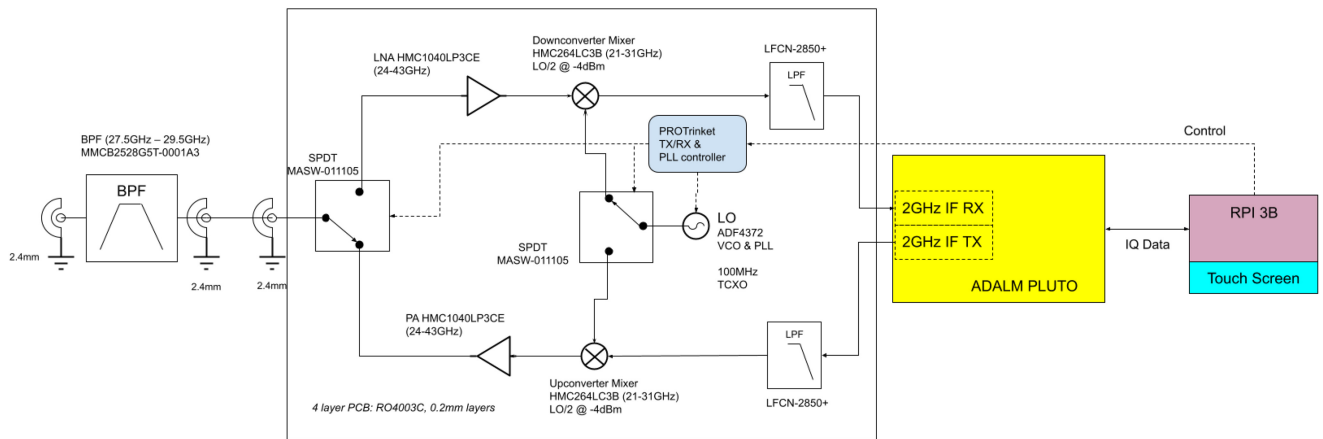
FIGURE 1. Channel sounder system (two required: one as TX and one as RX).

test equipment is used and offers a 138–172-dB PL measurement capability. The authors observed an excess PL of up to 15 dB over FSPL expectations on LoS links.

Though the 28-GHz band is now important for 5G and future 6G links, there is little understanding of what the PL models look like when close-to-ground. Indeed, in general there are few reported results for radio systems operating close-to-ground, with most research focusing on mobile or fixed communication links involving a high base station. However, there has been some military interest in UHF operation close-to-ground. In [28] ultrawideband (UWB) channel soundings (3–10 GHz) are taken at antenna heights including 10 cm and 2 m over various distances to 200 m. RMS delay spread, and PL models are extracted.

Commercial lab equipment is used as the basis of the sounder and the TX and RX are linked by 200-m optical fibre for triggering. The authors report a strong dependence on antenna height to PL, with data fitted to log-normal models. In [29], 27.7-GHz channel models at up to 26 m, for radar and communications operation involving a vehicle are reported, using lab equipment and antenna heights of 0.3 and 0.5 m.

Measurements in the ISM bands (433/868/915/2400 MHz) are a common focus for near-ground propagation measurements. In [30], antenna heights of 50 cm are used in building corridors and compared to ray tracing models, with large differences seen compared to ITU models. Outdoor measurements for antennas at 5 cm to 1 m at 470 MHz are reported in [31] with data compared to reflective earth (RE) and log-normal shadowing loss models.

III. HARDWARE SYSTEM DESIGN

The developed 28-GHz propagation measurement system is shown in Fig. 1. To maintain flexibility for future applications, certain architectural decisions were made early in the design. In the receive mode, the incoming signals are routed through a single-pole–double-throw (SPDT) switch (Analog Devices MASW-011105) and LNA (Analog Devices HMC1040) and then downconverted to a software adjustable

2-GHz IF, by an Analog Devices HMC264 mixer. The IF signal is then routed out to the SDR RX port. On TX, the IF signal from the SDR is upconverted to 28 GHz by a HMC264, amplified by an HMC1040 and routed out through the MASW-011105 SPDT. The limiting component defining the hardware RF frequency range is the HMC264 mixer, which can operate between 21–31 GHz. By placing the band select filter outside of the transceiver allows this range to be maintained. The local oscillator for the transceiver is generated by an Analog Devices ADF4372 integrated voltage-controlled oscillator (VCO) and phase-locked loop (PLL). The PLL uses a 100-MHz temperature compensated crystal oscillator (TCXO) as Master reference. It will be noted that the PCB includes TX and RX functions, though in practice when used as a sounder only the TX or RX function is used. However, having both functions available offers flexibility during field trials, with either unit able to work as TX or RX. If costs are an issue, then the unwanted circuit functions (one amplifier and a mixer) could be unpopulated during assembly, resulting in a dedicated TX or RX build, for a £ 97 saving.

The TX/RX circuit control and PLL frequency control is implemented within the transceiver by a PROTrinket [32] with dedicated code. External control of the transceiver is then via a simple interface between a Raspberry Pi 3B with touch screen (R-Pi) and the PROTrinket. The TX sideband selection and RX band selection is implemented in an external BPF, which is on a separate PCB for flexibility. For this application, an MMCB2528G5T-0001A3 from TDK, covering 27.5–29.5 GHz was used. Although a 2-GHz IF is used, this could be reconfigured by changing the ADF4372 PLL register settings and IF low pass filters (LPFs) if necessary. The IF could be changed, if needed, to suit frequency ranges of alternative SDRs. The use of a 2-GHz IF here means the mixer image is 4 GHz away from the carrier and is properly removed by the external BPF. If a lower IF is used, care must be taken to manage the image susceptibility on RX and image generated on TX (which must be removed to keep emissions in-channel) through consideration of the external
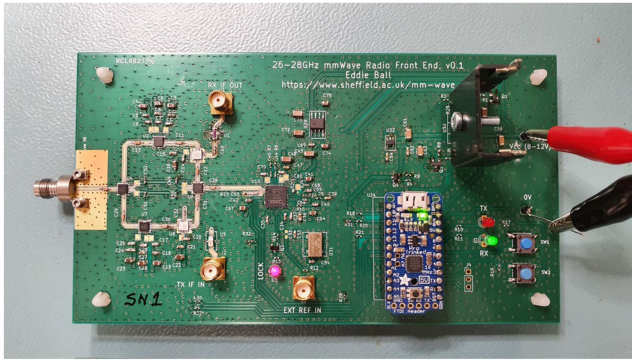
FIGURE 2. Fully assembled 28-GHz RF frontend PCB.

FIGURE 4. Example of enclosed system (box size 30 × 16 × 12 cm).
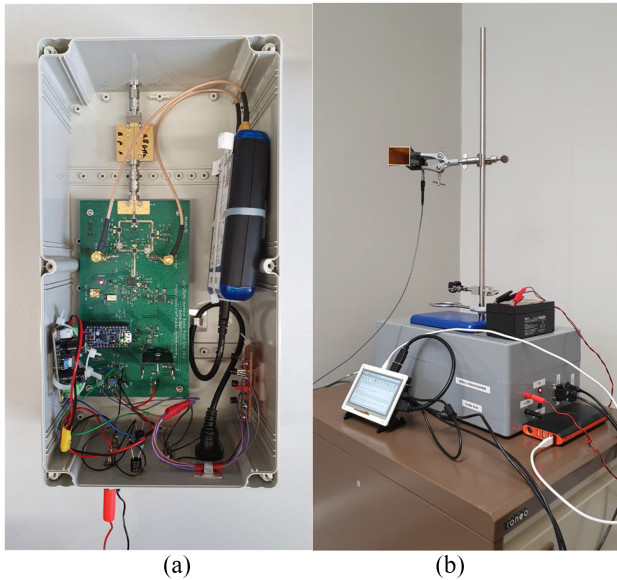

(a)   (b)

FIGURE 3. Sounder: (a) inside of a built sounder and (b) example sounder system.

BPF. Linear voltage regulators were used to generate the required circuit voltages. The PCB consists of four layers. Layers 1 and 2 use 0.2 mm of Rogers R4003C and layers 3 and 4 use 0.2-mm thick FR4.

The central FR4 prepreg core is 1.2 mm, resulting in a total unpopulated board thickness of 1.6 mm. The PCB size is 16.5 cm x 9 cm. An example of a built 28-GHz transceiver PCB is shown in Fig. 2. Design files for the PCB and PLL software can be obtained via [6]. To make a functional transceiver, a SDR platform and controller are required. In this project an ADALM Pluto [33] was used as the SDR and R-Pi with touch screen was used as the controller. R-Pi sounder analysis code was written in Python. An example completed sounder (RF PCB, external BPF, and SDR) is shown in Fig. 3(a). An example completed full sounder system is shown in Fig. 3(b): consisting of the sounder, R-Pi controller with touch screen and a 28-GHz horn antenna, with batteries. The small size of a built sounder is shown by Fig. 4, overall showing the system is easily hand portable. The PCB is powered at 6 V, which

avoids the chips running hot and needing external heatsinking. The RF chips have thermal paddles in their package—it is important these are properly soldered for RF ground and thermal dissipation to the PCB. The sounders have been operated continuously for over 4 hours, with only minor internal temperature rise observed. To protect the sounder from rain, there are no cooling holes in the case. Reproductions of the sounder equipment should properly consider heatsinking requirements for their own use cases—vent holes or metal enclosures may be beneficial.

At the time of writing, the cost of one fully assembled RF PCB was circa £ 1300 not including the SDR. Two test horn antennas were used (Quasar QWH21SB-UBR-K-F-20, with 17° beam width and 20-dBi gain), connected to the sounder using 2.4-mm connectorized coax cabling.

IV. SOUNDER ALGORITHM

The sounder uses a 511-bit PRBS modulated onto binary phase-shift keying (BPSK) transmitted data as the sounding signal. An efficient correlation procedure in the RX using circular convolution and FFTs [2] is used, based on (1)

$$C = \text{IFFT}\big[R(f)^*G(f)\big]. \tag{1}$$

In (1), $R(f)$ and $G(f)$ are the FFTs of RX time sample series $r(n)$ and prior known TX sequence $g(n)$, respectively, and * denotes complex conjugation. C is the resulting cross-correlation array of the time series and, thus, is the channel impulse response in the time domain. From this, the system can provide accurate measurements of RF power and RMS delay spread. The PRBS is modulated by the SDR as an IQ signal with chip rate of 30 Mchip/s, which is sufficient to illuminate a 60-MHz channel and resolve delays to 33 ns. The maximum-resolvable delay is 17 μs. Since there is no synchronization between the TX and RX, absolute channel delay cannot be measured. However, usually, in radio channel measurements, it is the channel frequency response and delay spread that is of primary interest, rather than absolute delay.

A. EQUALIZATION

The combined effect of the BPSK sinc shape of the TX sounding signal and the filters within the SDR RX chain require equalization before the measured channel spectral

TABLE 1. Equalization coefficients.

RX_{gain}	a	b	c	d	M_I	M_r
50	8.3×10^{-22}	-2.5×10^{-14}	2.3×10^{-07}	0.75	1.4×10^6	1.8
20	6.3×10^{-20}	-5.3×10^{-13}	1.5×10^{-06}	-0.13	5.5×10^6	1.7
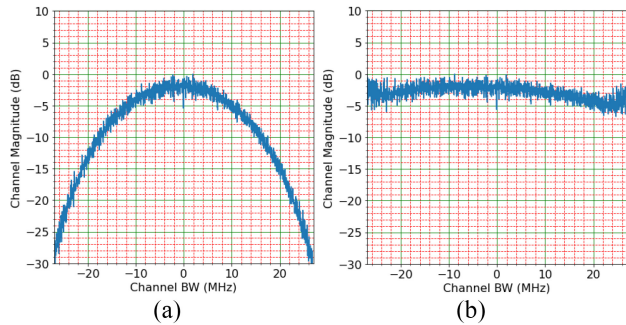
FIGURE 5. Example channel response equalization for BPSK sinc and hardware shaping effects: (a) no equalization applied and (b) equalization applied: only channel response of coax cable remaining.

response can be properly presented. This equalization is performed on the spectrum of the recovered RX signal, after using (1). The required spectrum amplitude equalization is calculated using (2), for FFT spectrum bin m out of N

$$\text{Eq}[m] = \left| \text{sinc}\left(\frac{m}{N}\right) \right|^r. \quad (2)$$

Coefficient r must be found and is a function of hardware imperfections. The correct value of r to use was found by laboratory experimentation using a PRBS-modulated RF signal generator at 28 GHz as the sounding source. The resolved spectrum from the sounder was monitored while r was adjusted, until r giving a flat resolved channel response is found. It was found that r was a mild function of the RX signal power and, hence, resolved impulse magnitude, so can be represented by a simple four term polynomial to scale the recovered spectrum (3), where x is the resolved impulse magnitude found in C using (1)

$$r = ax^3 + bx^2 + cx + d. \quad (3)$$

For high-impulse magnitudes beyond a level M_I, r can instead be fixed to a maximum value M_r using

$$\text{if } (x) > M_I \text{ then } r = M_r. \quad (4)$$

Two sets of coefficients are used, depending on which RX gain (RX_{gain}) is used by the SDR. Resulting found coefficient values used for (3) and (4) are shown in Table 1.

An illustration of the equalization action is presented in Fig. 5 showing the extracted channel response for an example PRBS modulated test signal (generated by a lab signal generator at 28 GHz, -75 dBm). Fig. 5(a) shows the channel response before equalization is applied, clearly showing the expected BPSK sinc shape dominating the spectrum plot. Fig. 5(b) shows the channel response after the equalization

is applied, with the sinc response now removed and the true channel response remaining (from a coax cable in this case). The flatness of the resolved channel, both before and after equalization, can be analyzed by considering the maximum and mean channel magnitude offsets from the ideal flat channel response of 0 dB (coax cable), over the full channel BW. Hence, in Fig. 5(a), before equalization, the mean offset is 7.5 dB and the max offset is 30 dB. In Fig. 5(b), after equalization, the mean offset is 1.0 dB and the max offset is 4.5 dB—both showing significant improvement due to the equalization.

B. SIGNAL LEVEL AND SDR RX_{GAIN}

During lab commissioning, it was found that two gain settings were required for the RX SDR, RX_{gain}, to achieve best measurement dynamic range (DR). The required gains are $RX_{gain} = 50$ for normal RX measurement from -110 to -45 dBm (theoretical FSPL distances $\sim$5 km down to $\sim$6 m). For short range measurements, $RX_{gain} = 20$ is suitable between -90 and -30 dBm (FSPL distances $\sim$1 km down to 1 m). This lower gain setting is useful for initial lab calibration and tests prior to commencing a field trial.

Accurate RX power received signal strength indication (RSSI) readings are very important and a key output from the channel sounder. The output from (1) represents an accurate measurement of the resolved impulse amplitude, for a given RX input PRBS-modulated carrier power. However, due to the frequency-dependent RF hardware gain and cable losses, etc, a correction factor is needed to relate (1) back to an RF power in dBm as seen at the test port. Hence, the actual received signal power is related to the resolved impulse magnitude x from C in (1) using

$$\text{RSSI} = RX_{powescale} \cdot 20 \log_{10}(x) + RX_{poweroffset} \text{ dBm} \quad (5)$$

where $RX_{powescale}$ is approximately 1 and $RX_{poweroffset}$ approximately -180 for an RX_{gain} of 20 and approximately -200 for an RX_{gain} of 50. Parameter $RX_{powescale}$ and $RX_{poweroffset}$ values also depend on specific channels used and so are found during initial lab commissioning calibration. This is done using a PRBS modulated sounder signal applied from a calibrated RF signal generator. Several RF test powers are applied across the DR of the sounder and, hence, the parameters for (5) are directly found. This calibration step needs only performing once, during equipment commissioning.

C. CARRIER ALIGNMENT

It is important that the TX and RX systems are carrier aligned before a sounding event commences. The alignment is done by setting up the TX unit to produce a CW tone on the desired channel and then setting up the RX system to receive on the same channel, in CW mode. The RX sounder then uses an FFT to find the carrier center and, hence, evaluate the overall carrier error. The found carrier error is then used by the sounding RX system to correct for all subsequent PRBS-based soundings.

TABLE 2. Theoretical and measured RF PCB performance.

Metric	Theoretical Design	Lab Measurements	
RX SSB NF	6.6	8.7	dB
TX gain	9	9	dB
RX gain	9	10	dB
RX IPP1dB	-15	-14	dBm
TX OPP1dB	6.2	1.0 DSB (*implies 4.0 dBm for SSB*)	dBm
RX BW	$21-31$ GHz	-	GHz
TX BW	$21-31$ GHz	-	GHz

The following channels were identified during commissioning and are selectable in the system: ch1 (27 GHz), ch2 (28 GHz), ch3 (29 GHz), ch4 (27.2 GHz), ch5 (27.5 GHz), and ch6 (27.65 GHz). In the U.K. ch2 and ch3 require an Ofcom Innovation and Trial Licence, but all other channels are in license exempt spectrum.

V. SYSTEM VERIFICATION TESTS

Two RF PCBs were built, commissioned, and tested for basic RF performance before integrating into the sounder system. An external switched mode buck converter was used to reduce the 12 V from the battery to 6 V for the PCB. The current drawn from the 12-V battery was 300 mA in both RX and TX modes. A 7-Ahr sealed lead acid battery is used to power the RF hardware during field operations, which should provide a service life of over 20 h. The key metrics for the version 0.1 PCB design are reported in Table 2.

The results in Table 2 are without the 28-GHz BPF fitted. It will be noted that the TX output 1-dB compression point (OPP1dB) is 5 dB lower than expectation and this is in part due to the lack of image filtering before the output stage; hence, the output amplifier will limit on the total applied RF power from both mixer sidebands (i.e., double sideband—DSB). If an image reject filter had been fitted prior to the amplifier then circa 3-dB improvement would be possible (hence single sideband (SSB) figure also quoted), however this would require the filter to be mounted on the PCB and would limit system flexibility for future use. Therefore, the necessary sideband selection filter is fitted at the output of the radio, as a separate PCB that is easy to swap. If higher TX powers are required, an outboard PA can then be fitted after this BPF. It will also be noted that the RX noise figure (NF) is 2 dB worse than predictions, possibly due to power supply noise and the losses from 2.4-mm connectors and adapters used in the sounder.

However, overall, the RF frontend is close to predictions for the line-up and is suitable for generic 28-GHz use.

A. TX POWER AND RX SENSITIVITY LAB VERIFICATION

Next, the RF PCB was connected to the SDR and 28-GHz input BPF and the effective sounder operational RF performance measured. The SDR was configured to generate an IF TX power of -10 dBm, which places the TX IF input 2 dB below the PCB TX input 1-dB compression point.
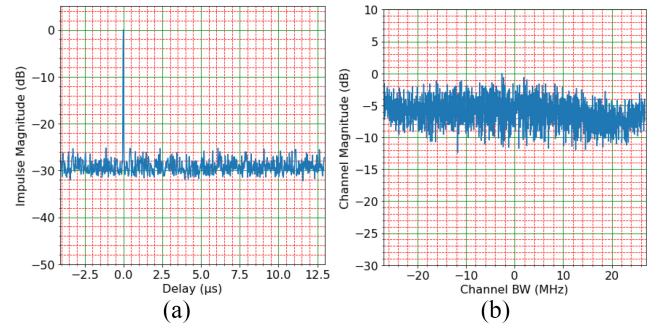
FIGURE 6. Channel 5 (27.5 GHz) RX at -80 dBm using signal generator source: (a) time-domain impulse and (b) channel frequency response.
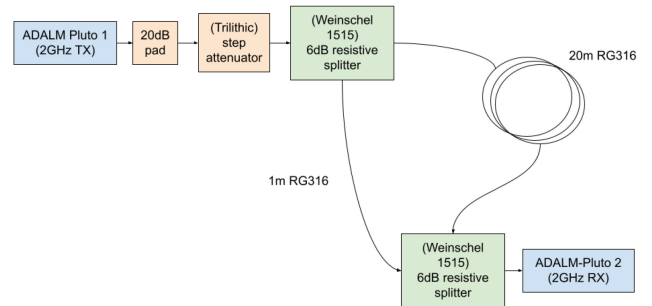
FIGURE 7. Reflection emulation using coax delay line, for tests at the SDR IF.

Two systems were tested for RX level measurement accuracy, using a Rohde & Schwarz SMW100A dual arbitrary waveform signal generator (transmitting the sounder 30 Mchip/s PRBS). Testing showed good agreement between applied RF PRBS modulated power and sounder resolved power between -30 and -110 dBm over all channels. Resolved mean RF power error is better than 0.7 dB and worst case error is 2 dB, for resolved impulse signal to measurement noise floor (SNR) ratios greater than 4 dB.

Channel 1 was found to be susceptible to a clock spur at the RX IF, radiating from the R-Pi CPU, so was not used in the field. The expected impulse SNR is limited by the length of the PRBS sequence and is 27 dB for a 511 chip length sequence. An example time-domain impulse and channel response from the tests are shown in Fig. 6.

The full sounder TX operation was also tested in the lab, with the conducted powers across all channels found to be between -8 and -10 dBm, apart from channel 3 at -19 dBm on both units. Additional loss was due to the BPF and associated cabling and adapters. The observed TX spectrum showed BPSK nulls at $+/-30$ MHz as expected for the PRBS chip rate. The 20-dB BW is 54 MHz, which represents a practical limit to the measured spectrum than can be equalized.

B. REFLECTION EMULATION USING COAXIAL CABLE DELAY

To confirm the sounder algorithm worked correctly with the SDR platform, a reflection path at the 2-GHz IF was emulated using a 1 and 20-m length of RG316 coax (velocity
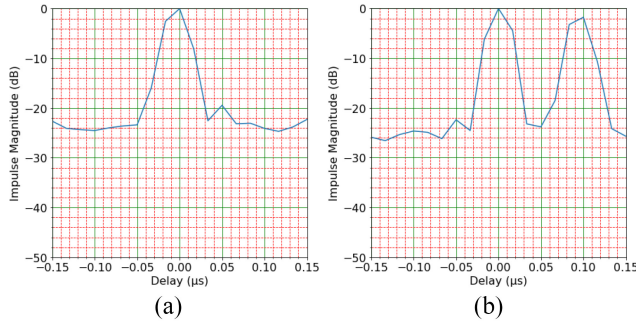
FIGURE 8. Zoomed-in view of impulse for (a) 1 m and (b) additional 20-m line, showing expected 95-ns delay due to additional coax path.
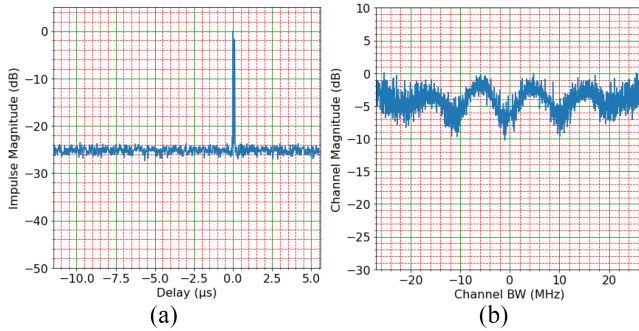

FIGURE 10. TX system during indoor soundings at The University of Sheffield.

FIGURE 9. Impulse response for test delay (a) time domain and (b) frequency domain, showing expected 11-MHz nulls due to coax cable lengths.

FIGURE 11. Outdoor field tests site with wet road (1-km testable distance).

factor∼ 0.7) combined using resistive splitters and combiners, as shown in Fig. 7. The resolved time-domain impulse for the single 1-m cable is shown in Fig. 8(a) and when the 20-m line is added in Fig. 8(b), clearly showing the two correlation peaks separated by 95 ns as expected.

The full time-domain impulse response (with the two impulses) is shown in Fig. 9(a) and the resolved frequency response in Fig. 9(b), which shows periodic nulls at 11 MHz, as would be expected for a 95-ns path delay difference.

VI. PROPAGATION SOUNDER FIELD TESTS

The sounder system was then tested in two scenarios, involving close-to-ground propagation. An indoor test and outdoor test were performed.

A. FIELD TEST SITES

As a first test, indoor channel soundings were performed in the Mappin Building at the University of Sheffield, at various points (nine locations, six localized tests per location) along a 100-m corridor, with TX test setup shown in Fig. 10. The horn antennas were both 70 cm above the corridor floor. All corridor obstructions were removed and all doors in the corridors were open.

Extended outdoor field tests were then conducted at a site on the outskirts of Doncaster in the U.K. (Lat.: 53.5222, Long: −1.0963), with the horn antennas 0.7 m above wet road and rough ground and with an overall testable distance of 1 km (21 test locations, three localized tests per location).

Fig. 11 shows the test road surface. The TX system was set up at the side of the road with visibility down the road. The RX system was moved along the road using a small hand trolley, as also shown in Fig. 10. Results from the two measurement sites are presented in the following sections.

Collected data is compared to a simple FSPL model (6), and where appropriate a simple RE with single reflected ray model (7), with antenna height above ground h, measured distance d and wavelength λ

$$PL_{\text{FSPL}} = 20\log_{10}\left(\frac{4\pi d}{\lambda}\right) \text{ dB} \tag{6}$$

$$PL_{\text{RE}} = 40\log_{10}(d) - 20\log_{10}\left(h^2\right) \text{ dB}. \tag{7}$$

Data is fitted to a standard log-normal PL model of form shown in (8) where n is the distance log-scaling term and K the fixed offset (corresponding to a reference distance of 1 m)

$$PL_{\text{model}} = n\log_{10}(d) + K + X_{\sigma} \text{ dB}. \tag{8}$$

Parameter X is a normal random variable with standard deviation σ dB for log-normal shadowing, calculated using (9), where N is the number of data points, PL_{data} is the PL measured, and PL_{model} is the PL predicted by (8) with X_{σ} set to zero

$$\sigma = \sqrt{\frac{1}{N}\sum_{k=1}^{N}\{PL_{\text{data}}(k) - PL_{\text{model}}(k)\}^2}. \tag{9}$$
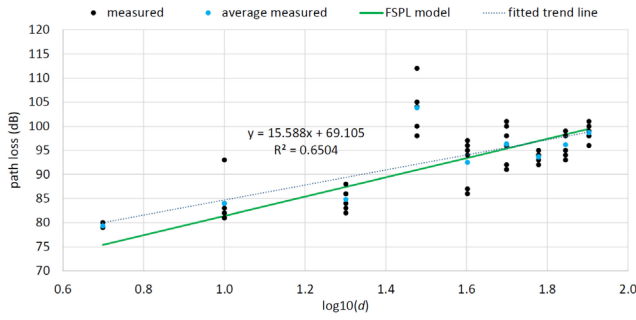
FIGURE 12. Extracted PL for 100-m in-building corridor: measured and FSPL comparison.

A sounding test takes under 1 min per location. Multiple readings were taken at each measurement location.

B. INDOOR PROPAGATION TEST RESULTS

Extracted PL results from the Mappin indoor corridor test are shown in Fig. 12, compared to FSPL model (6). The PL data has been fitted to the log-normal model (8) with a 1-m reference distance, resulting in

$$\text{PL}_{\text{corridor}} = 15.6\log_{10}(d) + 69.1 + X_{\sigma\_c} \text{ dB}. \quad (10)$$

For the corridor measurement results $\sigma\_c = 5.5$ dB. The fixed loss from a FSPL model at 1 m would be 61.4 dB. Thus, from (10), it can be seen that the fixed term K is 7.7 dB higher than for FSPL. In (10), it can also be seen that the fitted PL exponent n is 15.6, which is lower than expected for FSPL.

This perhaps suggests that the wave is acting as if in a lossy waveguide formed by the corridor. Similar effects have been seen by [18].

However, it is proposed that FSPL is a reasonable approximation to the corridor measurements since the overall PL is within 5 dB of FSPL. Brief testing was also conducted to assess the extra loss due to closing one set of wooden fire doors. The additional loss was measured at 19 dB and also a second impulse from a delayed ray at 88 ns was seen. Reflections were seen on some of the corridor measurements, though generally more than 20 dB below the main ray. However, the most notable reflections were around the 30-m point, with an example shown in Fig. 13. This also corresponds to the anomalous channel loss seen at $\log 10(d) = 1.48$ on Fig. 12. A visual inspection of the corridor area showed no environmental causes for this anomalous high PL. During subsequent analysis of the geometry of the test setup, it was calculated that destructive interference from a simple two-ray model of ground reflection could be expected close to 30 m and so could explain this result.

There are clearly several strong time-domain reflections present on Fig. 13(a), spreading across 500 ns (producing an RMS delay spread of 70.2 ns calculated using [2]). The spectral nulls caused by these reflections are seen in Fig. 13(b). Moving the sounder by 10 m moved it out of the reflective
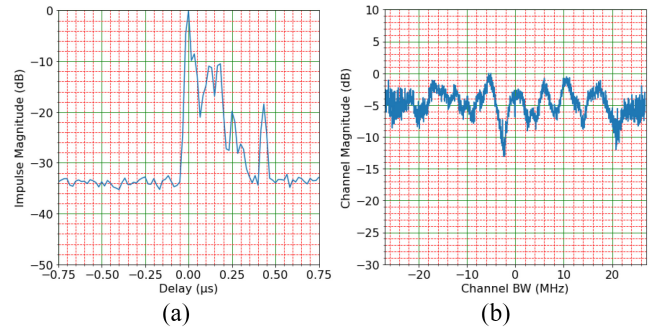

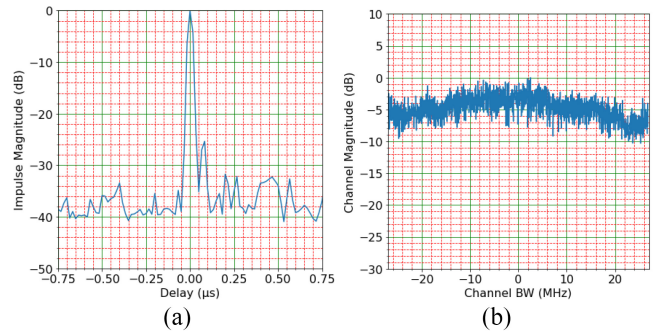**FIGURE 13.** Impulse response at 30-m range: (a) time domain and (b) spectrum.

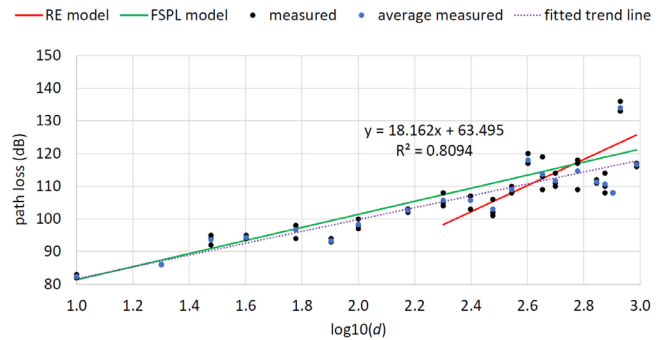**FIGURE 14.** Impulse response at 80-m range: (a) time domain and (b) spectrum.

FIGURE 15. Extracted PL for wet road & rough ground over 1 km, compared to RE and FSPL models.

area. For comparison, the channel response close to the end of the corridor is shown in Fig. 14.

C. OUTDOOR PROPAGATION TEST RESULTS

Outdoor tests were conducted over the 1-km LoS range. The TX was at a fixed site and the RX system was moved on a trolley to each test location, along a tarmac road. From Fig. 15, the extracted PL model is very close to that expected for FSPL, suggesting any reflections are minimal. A purely RE $40\log(d)$ model becomes valid after the first Fresnel zone distance of 183 m and is shown along with an FSPL model on Fig. 15. Although the data becomes more variable at this point, it still seems to approximate to the FSPL model.

The large increase in PL at 850 m (penultimate set of points) on Fig. 15 was caused by the path being obscured by several tree trunks after a bend in the road. A short
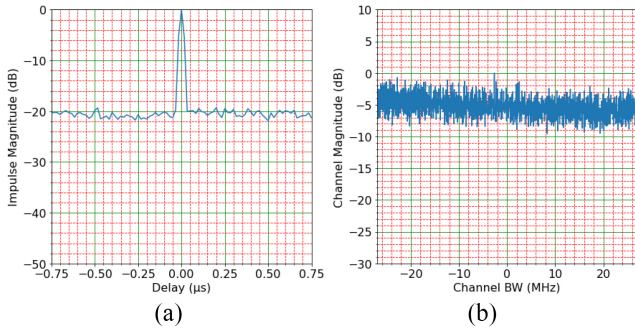
FIGURE 16. Impulse response at 971-m range: (a) time domain and (b) spectrum.

TABLE 3. Comparison of sounder performance to published works.

Ref	MPL (dB)	Equipment	RDR (ns)	DR (dB)	SRL (S)	TX BW (MHz)
[10]	-	USRP	10	-	-	100
[11]	145	lab kit	4	-	-	500
[12]	168	lab kit	2.3	-	-	800
[15]	170	lab kit	-	-	-	-
[16]	171	modules	-	75	-	CW
[17]	142	lab kit	1	-	-	1000
This Work	142	PCB, SDR & R-Pi	33	80	40	60

distance further along the road and a move onto some rough ground returns the link to LoS and the improvement in PL is seen for the final reported result set (corresponding to 800 m over tarmac and then 170 m over wet rough ground). The PL data has been fitted to the log-normal model (8), resulting in

$$\text{PL}_{\text{outdoor}} = 18.2\log_{10}(d) + 63.5 + X_{\sigma\_r} \text{ dB.} \quad (11)$$

From the measurement results, $\sigma\_r = 5.4$ dB. The fixed loss from an FSPL model at 1 m would be 61.4 dB and it can be seen in (11) that this is now within 2.1 dB of the model. It can also be seen that the log-exponent of 18.2 is also close to the 20 expected for FSPL. Overall, the measured data agrees well with an FSPL model.

A lack of resolvable reflections throughout the trial was confirmed by inspecting the time-domain impulse data. An example for the measurements at 971 m is shown in Fig. 16, showing a single resolved impulse and a flat channel (within the 60-MHz BW measurement capability).

Since the loss model (11) seems to fit an FSPL approximation, this also suggests that there is no polarization rotation over the tested distance.

It is also worth noting that the resolved impulse in Fig. 16(a) is 20 dB above the system measurement floor, suggesting that significant further distances could have been tested, though suitable field sites become hard to find in practice.

VII. DISCUSSION

The sounder and the related recent field test results will now be considered in the context of the prior works. A brief comparison of the sounder system performance to existing published sounders is presented in Table 3; considering max PL (MPL), reflection delay resolution (RDR), DR, sounding results latency (SRL), and TX sounding BW, where reported.

In [10], a USRP-N210 with 12.5-MHz sounding BW is expanded to an effective BW 100 MHz and 10-ns delay resolution through the use of repeated and overlapping OFDM sounding pattern, though MPL is not reported. Since the instantaneous sounding BW at 2.2 GHz is still limited to 12.5 MHz, any fast artifacts could be missed, since 100 MHz is not the instantaneous full sounding BW. The RF front end PCB created as part of this article could be used to extend the carrier frequency of the USRP or similar systems, if

desired. In our proposed system, the full 60-MHz channel is sounded instantaneously at 28 GHz.

A limitation of all other reported systems is the need for a PC to control and post-process the data (hence imposing measurement latency and potentially cumbersome in the field). Many of the reported systems use trolleys with mains powered equipment [11], [12], [13], [14], severely limiting mobility and suitability for outdoor use in complex environments. Expensive lab equipment would be risky and inconvenient to move to field test sites in bad weather and powering would bring safety concerns. The proposed system is easily hand portable, fully self-contained using commercially available ICs and produces channel frequency response and impulse delay spread measurement graphs on the touch screen within 40 s of the start of a sounding event (or 30 s if graphs not required) with no need for further data post processing. The compact and light-weight nature of the sounder, as seen in Fig. 4, could even support carriage by a suitably equipped drone, enabling many novel use-cases.

The use of circular convolution in (1) enables use of efficient FFT implementations in Python; hence, the good achieved execution time. This rapid operation in the field allows direct insight into propagation effects during a field trial. This feature was beneficial during our outdoor field trials, allowing visual investigation of the channel environment when unusual results were observed and, hence, guiding retries.

Although 1-ns reflection resolution is provided by Al-Samman et al. [17], this needs high-performance and cumbersome lab signal generators. In-building measurements in [18], [19], [20], and [25] similarly rely on high specification, large lab kit. In contrast, the reported system here uses a bespoke designed 28-GHz PCB that is cost effective, compact, and can be battery powered. The system can resolve a discrete reflection down to 33 ns (limited by the SDR), which is sufficient to resolve a delay path delta of 10 m—sufficient for many large spaces. The proposed system has a measurement BW of 60 MHz (limited by the SDR) and is not a limitation of the RF PCB. A 60-MHz BW may be suitable for many IoT applications. The RF front end PCB has a modulation BW that covers 21–31 GHz, hence significantly wider channel illumination is possible, if a suitable SDR platform is available. As is, the presented PCB 2-GHz IF could support a sounding BW of up to 2 GHz, if suitable RF BPFs are used, which would be the widest of the

sounders reported. The sounding algorithm is agnostic of SDR and could easily be adapted for different SDRs.

Lab trolley-based equipment in [15] offers a 170-dB PL capability and [16] uses CW to achieve 171 dB, though without delay spread capability. In [27], CW test kit supports a measurement budget of 138–172 dB, without delay spread capability. Although our system has a link budget limit of 142 dB, (though similar to [11] and [17]) this does provide time-domain delay spread measurements and was sufficient to measure to 1 km (and potentially beyond), in an outdoor LoS scenario. Link budget capability could be enhanced using an external RF PA to boost the TX power. For example, an external PA with gain of 20 dB would increase the TX power from -10 to $+10$ dBm and, thus, offer a 162-dB link budget. Additionally, a longer PRBS sounder sequence could be used—offering improved processing gain, though carrier lock may become necessary to avoid the PRBS sequence rotating in carrier phase over long duration sequences, if the oscillators drift.

At 80 dB, the proposed system has the best DR reported, representing beneficial tolerance of strong and weak signals during sounder operation. Unlike some other reported systems, the RF system developed has been fully characterized and full RF performance is reported. The use of sinc equalization on the extracted spectrum, to compensate for both the BPSK sounding signal and also RF hardware shaping effects, is very beneficial in maximizing resolvable channel BW.

There is also importance in the field test results reported here using the instrument. The work in this article is, to the best of our knowledge, the first set of published data for propagation models within 1 m of ground at 28 GHz over rough ground outdoors at long distance. The prior work by Sangodoyin et al. [28] studied UWB frequencies to 10 GHz and only to 200 m, while requiring a fibre link for triggering and not reporting channel response spectral shape. In contrast, we measure to 1 km and at 28 GHz without need for external synchronization and report channel spectral features where notable. The upper measurement frequency of [28] is 10 GHz and our measurements at 28 GHz represent a significant shift in frequency band, requiring revised models. The UWB PL exponent reported in [28] varies considerably between antennas at 50-cm heights ($n = 33.0$) and 2-m heights (closer to FSPL at $n = 21.4$)—hence, the importance of our results showing that at 28 GHz for 70-cm heights, the outdoor PL is closer to FSPL at $n = 18.2$. This is a key result and suggests the higher carrier frequency we have tested offers an advantage for close-to-ground operation. The shadowing model parameter in [28] is 2.8 dB for antennas at 2 m and 4.39 dB for antennas at 50 cm, whereas in our outdoor 28-GHz tests, we extracted a shadowing parameter value of 5.4 dB, again showing the importance of band-specific testing. Solomitckii et al. [29] studied channel models only to 26 m.

Measurement campaigns and models for propagation are always most relevant when in the direct band of interest, capturing all dependencies of the environment. The finding that outdoor PL, when close to ground, approximates FSPL

is quite surprising and was only possible thanks to the equipment's mobility. Similarly, the indoor model's closeness to FSPL with few reflections also suggests simple link budget models may be valid for many use cases.
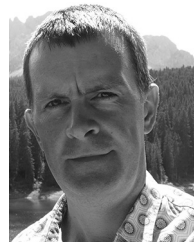
VIII. CONCLUSION

A bespoke 28-GHz hardware platform consisting of a custom designed mmWave RF PCB and commercial SDR, both controlled by an R-Pi, is presented and described in the context of a channel sounder. The sounder hardware is low-cost (£ 1300 for PCB & RF hardware) and the PCB design has been made available online to assist other researchers in the discipline, for their own adaptation and use. The sounder system is then used in two close-to-ground applications to measure PL and inspect channel impulse responses.

Extracted log-normal models are provided for the measured propagation data, with measurements showing PLs close to FSPL can be achieved at antenna heights of 0.7 m for indoor and outdoor LoS tests. Apart from the one location-specific case during the indoor corridor testing, there were no reflection paths observed exceeding the system's minimum resolvable 33 ns, further suggesting the suitability of the FSPL model, at least for the tested BW. Overall, this suggests that unobstructed mmWave signal transmission close-to-ground is entirely viable over communications BWs of circa 60 MHz. This could be useful for covert or low probability of intercept communication applications.

REFERENCES

[1] C. Casetti, "The challenges of universal broadband connectivity [mobile radio]," *IEEE Veh. Technol. Mag.*, vol. 17, no. 3, pp. 5–11, Sep. 2022, doi: 10.1109/mvt.2022.3176414.

[2] E. A. Ball, "Design and field trial measurement results for a portable and low-cost very-high-frequency/ultra-high-frequency channel sounder platform for Internet of Things propagation research," *IET Microwaves Antennas Propag.*, vol. 13, no. 6, pp. 714–724, May 2019, doi: 10.1049/iet-map.2018.5827.

[3] D. P. Wright and E. A. Ball, "Highly portable software defined radio test bed for dual band propagation studies," in *Proc. Loughborough Antennas Propag. Conf. (LAPC)*, 2018, pp. 1–6, doi: 10.1049/cp.2018.1472.

[4] D. P. Wright and E. A. Ball, "IoT focused VHF and UHF propagation study and comparisons," *IET Microwaves Antennas Propag.*, vol. 15, no. 8, pp. 871–884, 2021, doi: 10.1049/mia2.12101.

[5] T. S. Rappaport, G. R. MacCartney, M. K. Samimi, and S. Sun, "Wideband millimeter-wave propagation measurements and channel models for future wireless communication system design," *IEEE Trans. Commun.*, vol. 63, no. 9, pp. 3029–3056, Sep. 2015, doi: 10.1109/TCOMM.2015.2434384.

[6] "RF PCB Files." Accessed: Sep. 1, 2022. [Online]. Available: https://www.sheffield.ac.uk/mm-wave/futuremmwave/downloads-pcb-design-files

[7] Y. Wang, Y. Lv, X. Yin, and J. Duan, "Measurement-based experimental statistical modelling of propagation channel in industrial IoT scenario," *Radio Sci.*, vol. 55, no. 9, pp. 1–14, Sep. 2020, doi: 10.1029/2019RS007013.

[8] Y. Lyu, A. W. Mbugua, Z. Yuan, K. Olesen, and W. Fan, "Design and validation of a multilink phase-compensated long-range ultrawideband VNA-based channel sounder," *IEEE Trans. Microw. Theory Techn.*, vol. 70, no. 10, pp. 4528–4543, Oct. 2022, doi: 10.1109/TMTT.2022.3194045.

[9] S. Salous, A. Cheema, and X. Raimundo, "Radio channel propagation measurements using a multiband agile chirp sounder," in *Proc. 31st URSI Gen. Assembly Sci. Symp.*, 2014, pp. 1–4, doi: 10.1109/URSIGASS.2014.6929650.

[10] B. B. Harianto, M. Hendrantoro, G. Ardiansyah, and A. Mauludiyanto, "Measurement of wideband indoor radio propagation channel using USRP," *J. Phys. Conf.*, vol. 1381, no. 1, pp. 1–10, Nov. 2019, doi: 10.1088/1742-6596/1381/1/012054.

[11] J. Ko, S. U. Lee, Y. S. Kim, and D. J. Park, "Measurements and analyses of 28 GHz indoor channel propagation based on a synchronized channel sounder using directional antennas," *J. Electromagn. Waves Appl.*, vol. 30, no. 15, pp. 2039–2054, Oct. 2016, doi: 10.1080/09205071.2016.1239552.

[12] M. Samimi et al., "28 GHz angle of arrival and angle of departure analysis for outdoor cellular communications using steerable beam antennas in New York City," in *Proc. IEEE Veh. Tech. Conf.*, Dresden, Germany, 2013, pp. 1–6, doi: 10.1109/VTCSpring.2013.6691812.

[13] H. Zhao et al., "28 GHz millimeter wave cellular communication measurements for reflection and penetration loss in and around buildings in New York City," in *Proc. IEEE Int. Conf. Commun.*, Budapest, Hungary, 2013, pp. 5163–5167, doi: 10.1109/ICC.2013.6655403.

[14] Y. Azar et al., "28 GHz propagation measurements for outdoor cellular communications using steerable beam antennas in New York City," in *Proc. IEEE Int. Conf. Commun.*, Budapest, Hungary, 2013, pp. 5143–5147, doi: 10.1109/ICC.2013.6655399.

[15] J. Lee, J. Liang, J.-J. Park, and M.-D. Kim, "Beamwidth-dependent directional propagation loss analysis based on 28 and 38 GHz urban micro-cellular (UMi) measurements," in *Proc. IEEE 86th Veh. Technol. Conf. (VTC-Fall)*, Toronto, ON, Canada, 2017, pp. 1–5, doi: 10.1109/VTCFall.2017.8288370.

[16] J. Du et al., "Directional measurements in urban street canyons from macro rooftop sites at 28 GHz for 90% outdoor coverage," *IEEE Trans. Antennas Propag.*, vol. 69, no. 6, pp. 3459–3469, Jun. 2021, doi: 10.1109/TAP.2020.3044398.

[17] A. M. Al-Samman, T. A. Rahman, M. H. Azmi, and S. A. Al-Gailani, "Millimeter-wave propagation measurements and models at 28 GHz and 38 GHz in a dining room for 5G wireless networks," *Measurement*, vol. 130, pp. 71–81, Dec. 2018, doi: 10.1016/j.measurement.2018.07.073.

[18] A. M. Al-Samman, T. A. Rahman, and M. H. Azmi, "Indoor corridor wideband radio propagation measurements and channel models for 5G millimeter wave wireless communications at 19 GHz, 28 GHz, and 38 GHz Bands," *Wireless Commun. Mobile Comput.*, vol. 2018, pp. 1–13, Mar. 2018, doi: 10.1155/2018/6369517.

[19] S. Ju, Y. Xing, O. Kanhere, and T. S. Rappaport, "Millimeter wave and sub-terahertz spatial statistical channel model for an indoor office building," *IEEE J. Sel. Areas Commun.*, vol. 39, no. 6, pp. 1561–1575, Jun. 2021, doi: 10.1109/JSAC.2021.3071844.

[20] M. A. Samad, F. D. Diba, Y. J. Kim, and D. Y. Choi, "Results of large-scale propagation models in campus corridor at 3.7 and 28 Ghz," *Sensors*, vol. 21, no. 22, p. 7747, Nov. 2021, doi: 10.3390/s21227747.

[21] G. Zhang et al., "Experimental characterization of millimeter-wave indoor propagation channels at 28 GHz," *IEEE Access*, vol. 6, pp. 76516–76526, 2018, doi: 10.1109/ACCESS.2018.2882644.

[22] S. Nie, G. R. MacCartney, S. Sun, and T. S. Rappaport, "28 GHz and 73 GHz signal outage study for millimeter wave cellular and backhaul communications," in *Proc. IEEE Int. Conf. Commun. (ICC)*, Sydney, NSW, Australia, 2014, pp. 4856–4861, doi: 10.1109/ICC.2014.6884089.

[23] D. He et al., "Influence analysis of typical objects in rural railway environments at 28 GHz," *IEEE Trans. Veh. Technol.*, vol. 68, no. 3, pp. 2066–2076, Mar. 2019, doi: 10.1109/TVT.2018.2840097.

[24] G. R. MacCartney, T. S. Rappaport, S. Sun, and S. Deng, "Indoor office wideband millimeter-wave propagation measurements and channel models at 28 and 73 GHz for ultra-dense 5G wireless networks," *IEEE Access*, vol. 3, pp. 2388–2424, 2015, doi: 10.1109/ACCESS.2015.2486778.

[25] S. Ito and T. Hayashi, "Measurement and evaluation of 28 GHz propagation characteristics in specific environments," *IEEE Access*, vol. 10, pp. 26242–26256, 2022, doi: 10.1109/ACCESS.2022.3157063.

[26] J. Ko et al., "Measurements and analysis of radio propagation at 28 GHz in vegetated areas of typical residential environments," *IEEE Trans. Antennas Propag.*, vol. 68, no. 5, pp. 4149–4154, May 2020, doi: 10.1109/TAP.2020.2968801.

[27] J. Du, D. Chizhik, R. Feick, M. Rodriguez, G. Castro, and R. A. Valenzuela, "Suburban fixed wireless access channel measurements and models at 28 GHz for 90% outdoor coverage," *IEEE Trans. Antennas Propag.*, vol. 68, no. 1, pp. 411–420, Jan. 2020, doi: 10.1109/TAP.2019.2935110.

[28] S. Sangodoyin, S. Niranjayan, and A. F. Molisch, "A measurement-based model for outdoor near-ground ultrawideband channels," *IEEE Trans. Antennas Propag.*, vol. 64, no. 2, pp. 740–751, Feb. 2016, doi: 10.1109/TAP.2015.2505004.

[29] D. Solomitckii, V. Semkin, M. Turunen, M. Allén, and M. Valkama, "Near-ground propagation in automotive radar and communication obstructed deployments: Measurements and modelling," *IET Microwaves Antennas Propag.*, vol. 16, no. 6, pp. 316–326, May 2022, doi: 10.1049/mia2.12241.

[30] T. R. Rao, D. Balachander, T. Nishesh, and M. V. S. N. Prasad, "Near ground path gain measurements at 433/868/915/2400 MHz in indoor corridor for wireless sensor networks," *Telecommun. Syst.*, vol. 56, no. 3, pp. 347–355, Jul. 2014, doi: 10.1007/s11235-013-9848-1.

[31] W. Tang, X. Ma, J. Wei, and Z. Wang, "Measurement and analysis of near-ground propagation models under different terrains for wireless sensor networks," *Sensors*, vol. 19, no. 8, pp. 1–13, Apr. 2019, doi: 10.3390/s19081901.

[32] "Adafruit Ltd ProTrinket." Accessed: Sep. 1, 2022. [Online]. Available: https://learn.adafruit.com/introducing-pro-trinket

[33] "Analog Devices ADALM Pluto SDR." Accessed: Sep. 1, 2022. [Online]. Available: https://www.analog.com/en/design-center/evaluation-hardware-and-software/evaluation-boards-kits/adalm-pluto.html

EDWARD A. BALL (Member, IEEE) was born in Blackpool, U.K., in November 1973. He received the Master of Engineering degree (First Class) in electronic systems engineering from the University of York, York, U.K., in 1996.

After graduating, he worked in industry for 20 years, first spending 15 years working as an Engineer, a Senior RF Engineer, and finally a Principal RF Engineer with Cambridge Consultants Ltd., Cambridge, U.K. He then spent five years as a Principal RF Engineer and a Radio Systems Architect with Tunstall Healthcare Ltd., Whitley, U.K. He joined the Department of Electronic and Electrical Engineering, University of Sheffield, Sheffield, U.K., in November 2015, where he currently works as a Reader of RF Engineering. His research interests cover all areas of radio technology, from RF system design, RF circuit design (sub-GHz to mmWave), and the application of radio technology to real-world industrial and commercial problems. He has a particular passion for RF hardware design.

Mr. Ball is a member of IET and a Chartered Engineer.

SUMIN DAVID JOSEPH received the B.Tech. degree (Hons.) in electronics and communication from the Cochin University of Science and Technology, Cochin, India, in 2012, the M.Tech. degree (Hons.) in communication systems from the Visvesvaraya National Institute of Technology, Nagpur, India, in 2015, and the dual Ph.D. degrees (distinction) in electrical engineering from the University of Liverpool, Liverpool, U.K., and National Tsing Hua University, Hsinchu, Taiwan, in 2021.

He is currently working as a Postdoctoral Research Associate with The University of Sheffield, Sheffield, U.K. He was a Lab Engineer under CoE with the Visvesvaraya National Institute of Technology from 2015 to 2017, where he was involved in projects of national importance. He has authored or coauthored more than 25 articles in peer-reviewed journals and conference proceedings. His research interests include self-biased circulators, mmWave antenna arrays, rectifying antennas, MMIC circuit design, RF circuit design, rectifiers, integrated circuit designs, flexible electronics, wireless power transfer, energy harvesting, and TMA antenna arrays.

Dr. Sumin is a Technical Reviewer for leading academic journals and conferences, including the IEEE TRANSACTIONS OF ANTENNA AND PROPAGATION, IEEE ANTENNA AND WIRELESS PROPAGATION LETTERS, and IEEE ACCESS.